


Article

Monitoring Surface Deformation over a Failing Rock Slope with the ESA Sentinels: Insights from Moosfluh Instability, Swiss Alps

Andrea Manconi ^{1,*} , Penelope Kourkouli ^{1,2}, Rafael Caduff ², Tazio Strozzi ²  and Simon Loew ¹

¹ Department of Earth Sciences, Engineering Geology, Swiss Federal Institute of Technology, ETH Zurich, Sonneggstrasse 5, 8092 Zurich, Switzerland; penelope.kourkouli@erdw.ethz.ch (P.K.); simon.loew@erdw.ethz.ch (S.L.)

² Gamma Remote Sensing AG, Worbstrasse 225, 3073 Gümligen, Switzerland; caduff@gamma-rs.ch (R.C.); strozzi@gamma-rs.ch (T.S.)

* Correspondence: andrea.manconi@erdw.ethz.ch; Tel.: +41-44-663-8405

Received: 12 March 2018; Accepted: 23 April 2018; Published: 25 April 2018



Abstract: We leverage on optical and radar remote sensing data acquired from the European Space Agency (ESA) Sentinels to monitor the surface deformation evolution on a large and very active instability located in the Swiss Alps, i.e., the Moosfluh rock slope. In the late summer 2016, a sudden acceleration was reported at this location, with surface velocity rates passing from maximum values of 0.2 cm/day to 80 cm/day. A dense pattern of uphill-facing scarps and tension cracks formed within the instability and rock fall activity started to become very pronounced. This evolution of the rock mass may suggest that the most active portion of the slope could fail catastrophically. Here we discuss advantages and limitations of the use of spaceborne methods for hazard analyses and early warning by using the ESA Sentinels, and show that in critical scenarios they are often not sufficient to reliably interpret the evolution of surface deformation. The insights obtained from this case study are relevant for similar scenarios in the Alps and elsewhere.

Keywords: landslide deformation monitoring; radar interferometry; digital image correlation; rock slope failure

1. Introduction

The progressive evolution of a slope towards catastrophic failure is often associated to an exponential increase of ground displacements [1,2]. For this reason, accurate monitoring data of surface deformation in slope areas is a key to promptly identify spatial and/or temporal behavioral changes. Remote sensing techniques have demonstrated in recent years to be a valid complement to the standard in-situ monitoring techniques [3–6]. In particular, satellite based imagery allowed great advances in the identification, mapping, and quantification of surface deformation processes of slopes both at regional and local scales. An important technique to monitor slope displacement is spaceborne Differential Synthetic Aperture Radar Interferometry (DInSAR, [7]). This method can be used to measure ground deformation by relying on the phase difference between multi temporal SAR acquisitions, with accuracies in the range of mm to cm [5,8]. Some limitations on the use of DInSAR technique arise when the surface deformation is relatively large and rapid [9,10]. Indeed, when the deformation rate overcomes spatial and/or temporal aliasing thresholds, the coherence of the radar phase is not preserved and thus measurements are hindered [11]. This problem arises when a large deformation gradient affects relatively small areas, a characteristic scenario for slope instabilities

evolving towards failure [9]. Several authors have proposed to overcome this limitation by analyzing the amplitude information of SAR images with Digital Image Correlation (DIC) techniques [12–15].

This approach allows retrieving surface displacements also when large spatial gradients occur; however, accuracies are reduced compared with standard DInSAR approaches [11,16]. In addition to SAR imagery, optical and multispectral data acquired from a large number of orbiting satellites can be nowadays exploited to build time series spanning decades, and to detect surface changes associated to ground displacements [17,18]. Likewise, in this case DIC approaches can be used to quantify offsets caused by the deformation. This strategy was initially developed to study the rapid flow of large glaciers [19], but more and more often applied to slope instabilities and landslide events [20,21].

In general, spaceborne remote sensing data is considered to quantify surface displacements in back analyses, either over regional scale to map the active slope instabilities and assess hazard potential [22–24], or to perform forensic studies at the scale of a single slope shortly before/after a landslide failure event occurs [25,26]. However, systematic satellite acquisitions with revisit times and ground sampling distances suitable for slope instability monitoring are nowadays available. In particular, the European Space Agency (ESA) missions known as “Sentinels” developed within the operational needs of the Copernicus program, formerly GMES, can be considered as a real game changer [27]. In this work, we take advantage of the ESA Sentinel-1 (radar imagery) and Sentinel-2 (multispectral imagery) to study the evolution of a deep seated gravitational slope deformation (DSGSD) located in the crystalline basement of Swiss Alps, near the tongue of the Great Aletsch Glacier (see Figure 1). This area, hereafter referred to as the Moosfluh rock slope instability, has shown evidences of slow but progressive increase of surface displacements during the past 20 years from about 4 cm/year during the 1990’s to more than 20 cm/year in 2008 [6,28]. In the late summer 2016, a sudden acceleration was reported, with surface velocity rates reaching maximum values of about 80 cm/day. During the following winter (November 2016–March 2017) ground deformation decelerated, however, rates were still conspicuous compared with previous winter periods. The entire instability area developed a dense pattern of steeply dipping antithetic and synthetic scarps with in-plane shear of several meters and minor extension. In addition, large secondary scarps developed within the DSGSD (see Supplementary Materials, Figure S1). This evolution of the rock mass may suggest that a significant portion of the slope could fail [29]. The aim of this study is to investigate if spaceborne data acquired from the Sentinels are suitable to measure accurately surface deformation in a critical scenario of slope instability evolving towards a potential catastrophic failure event.

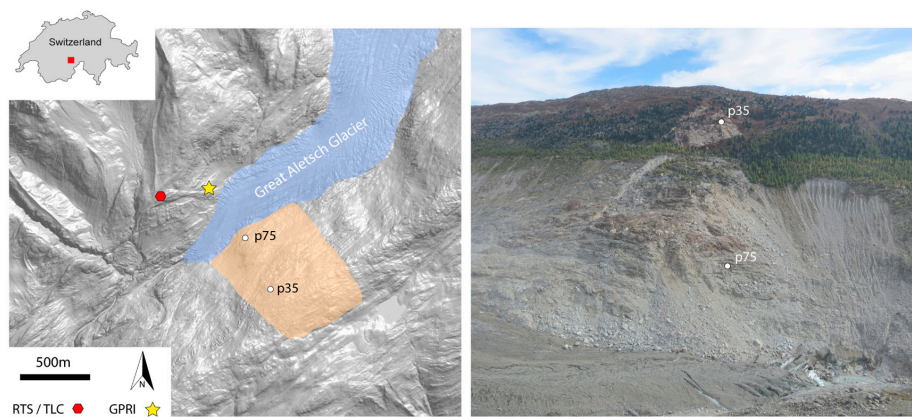


Figure 1. Geographic overview of the area of study, i.e., the Moosfluh rock slope instability located in the vicinity of the Great Aletsch Glacier, Swiss Alps. **(Left)** Moosfluh rock slope instability (orange shading) and Great (blue shading) on the hill shade model. The position of ground based monitoring instruments is also indicated, i.e., Robotized Total Station (RTS), Time Lapse Camera (TLC), and GAMMA Ground Portable Radar Interferometer (GPRI). **(Right)** Picture of the Moosfluh instability acquired on 28 September 2017 during the GPRI survey. The two points, p35 and p75, are reflectors (prisms) monitored hourly from the RTS. See text for more details.

2. Data and Methods

The ESA Sentinels are equipped with different technologies ranging from radar to multispectral sensors, and can be applied to monitor diverse parameters to characterize atmosphere, oceans, and land. Compared to previous space programs, the Sentinels are designed to provide unprecedented spatial coverage and revisit times. Sentinel-1 and Sentinel-2 constellations acquire data relevant to identify and measure surface deformation due to slope instability on Earth's surface, thus are relevant for our analyses.

Sentinel-1 is a C-Band radar-imaging mission (wavelength $\lambda = 5.6$ cm) composed of two satellites projected to study land and oceans [30]. Sentinel-1A (S1A) was launched on 3 April 2014 and Sentinel-1B (S1B) on 25 April 2016. S1 constellation provides multiple SAR image acquisition strategies. Among them, the TOPS Interferometric Wide swath (IW) acquisition mode has been specifically designed for DInSAR applications [31]. The combination of data acquired from S1A and S1B satellites provides almost global coverage of the Earth's surface and revisit times between 6 and 12 days (i.e., same area and same orbit path suitable for DInSAR). Ground sampling distances (GSD) are in the order of 2.3 m in range and 13.6 m in azimuth directions, respectively. Sentinel-2 is a multispectral high-resolution imaging mission composed also of twin satellites for land monitoring providing imagery of vegetation, soil and water cover, inland waterways and coastal areas [32]. Sentinel-2A (S2A) was launched on 23 June 2015 and Sentinel-2B (S2B) followed on 7 March 2017. S2 sensors provide 13 spectral bands ranging from visible to short-wavelength infrared (SWIR), with revisit times between 5 and 10 days (same orbit over the same area for comparative analyses) and GSD ranging from 10 to 60 m.

We considered 38 Sentinel-1 and 35 Sentinel-2 images acquired in the period of March–October, 2017, over the Moosfluh area (see also the Supplementary Materials, Tables S1 and S2). We focused our analysis on this specific time window to increase the chances of obtaining snow free imagery, but also because surface deformation at the Moosfluh rock slope increases in spring and early fall periods, and fades during summer and winter times [28]. This behavior was observed over several seasons with in-situ monitoring instruments and the underlying mechanisms are currently studied in detail. Spring acceleration of alpine DSGSD is usually explained in Moosfluh but also in other alpine rock slope instabilities as the effect of ground water pressure variations due to the infiltration of snow melt [1,28,33], however, the physical processes governing the accelerations in late summer

might be related to interactions with the valley glacier at the landslide toe. Here we measure surface deformation at Moosfluh with two approaches: (1) DInSAR analyses of the phase information of the Sentinel-1 dataset; (2) DIC applied to the SAR amplitude information of the Sentinel-1 dataset, and to the surface reflectance data of the Sentinel-2 dataset.

2.1. DInSAR Analysis

Considering the S1A and S1B imagery available and suitable to fully image displacements occurring in our study area (track 66, descending path, see also the Supplementary information, list of images), 67 differential interferograms were computed with the GAMMA software [34]. We have paired subsequent acquisitions to obtain the shortest possible temporal separation between SAR images (6 days) and thus minimize phase decorrelation effects due to temporal discrepancy (best case scenario). Moreover, we also generated interferograms with 12 days temporal baseline, to assess DInSAR results in a potential scenario of accelerated surface deformation in areas where the 6 days revisit time capabilities of Sentinel-1 are not available [30]. Because the average value and standard deviation of perpendicular baselines are 50 m and 38 m, respectively (see also Supplementary Materials, Table S3), SAR phase decorrelation in the interferograms is expected mainly due to disturbances occurring at the ground surface [35].

2.2. DIC Analysis

Digital Image Correlation analyses can be applied to measure sub-pixel misalignments potentially associated to surface deformation occurring parallel to the image plane. This converts to along-track (azimuth) and across-track (range) directions for Sentinel-1 radar data, and E-W and N-S motions for Sentinel-2 imagery. Considering the best Ground Sampling Distance (GSD) of Sentinel-1 and Sentinel-2 (i.e., GSD = 2.3 m in range direction and GSD = 13.6 m in azimuth direction for S1, Single-Look-Complex (SLC) data, and GSD = 10 m for S2 data), with the DIC analysis we expect to measure surface deformation in the order of decimeters to several meters [11]. Among several DIC methods developed to measure surface displacement from remote sensing imagery [36], here we selected the FFT based cross-correlation approach proposed by [37]. For S1 data, we relied on the SLC intensities (in slant-range) after performing an initial co-registration step to obtain a homogeneous alignment of the multitemporal SAR acquisitions [38]. Instead, for S2 data we used the Level 2A Bottom-Of-Atmosphere corrected reflectance product in ground geometry (B8 SWIR spectral band, central wavelength 842 nm).

For both S1 and S2 imagery, we applied an initial co-registration step to mitigate the effects of potential rigid shifts between master and slave imagery due to different acquisition parameters. Then, a correlation window size of 64×64 pixels with an oversampling factor $4\times$ was used to measure sub-pixel offsets due to deformation [39]. Image pairing strategy for S1 data followed the same approach applied for DInSAR (see Section 2.1). For what concerns S2 data, two adjacent paths covered the area of Moosfluh during the time period analyzed, i.e., tracks R108 and R065, both with revisit time of 10 days (see also Supplementary Materials, Table S3).

3. Results

3.1. Results of DInSAR Analyses

Figures 2 and 3 show a selection (one per month) of the differential interferograms computed with 6 days and 12 days separation (see also Supplementary Materials, Figure S2, for the full set of interferograms). In both figures, phase decorrelation effects are evident due to snow cover in pairs spanning March and April 2017, as well as due to the large changes affecting the surface of the Great Aletsch glacier. Focusing on the sequence with 6-days temporal sampling, deformation is well imaged in the upper portions (elevations between 2000 m and 2300 m a.s.l.) of the Moosfluh slope instability, with maximum values of about 0.03 m (one fringe) along satellite line-of-sight (LOS) at the end of

May 2017 (interferogram 27 May–2 June 2017). This converts to maximum surface velocities of about 0.005 m/day. When looking at the 12-day interferogram for the same temporal frame (interferogram 21 May–2 June 2017), we notice that spatial aliasing occurs because of the large surface velocities and thus deformation for this area is not measurable. LOS deformation fades out over time, approaching values of few millimeters towards the end of October 2017. Another important feature visible in both 6-days and 12-days interferograms, is the persistent decorrelation affecting the lower portions (between 1900 m and 2000 m a.s.l.) of the Moosfluh slope. In this area, surface velocities are too high to be imaged with standard DInSAR methods in our period of investigation.

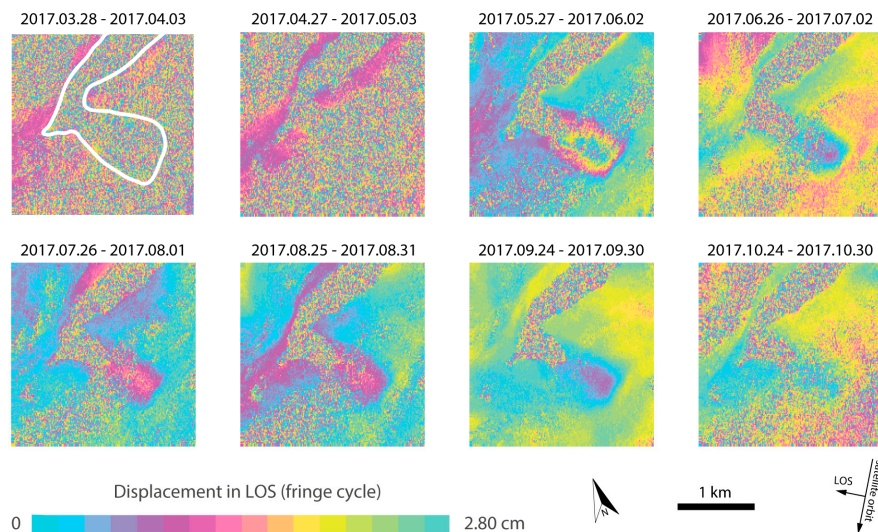


Figure 2. Selection of the Sentinel-1 (track 66, descending orbit) differential interferograms with 6-days temporal separation over the area of Moosfluh rock slope instability for the period March–October 2017. Time of acquisition for the SAR image pairs is provided in the format YYYY.MM.DD. White boundary in the upper left interferogram delineates the approximate area of the Aletsch glacier and Moosfluh slope instability (cf. Figure 1). Differential interferograms were generated by using a high resolution DEM (SwissALTI3D, 2 m GSD) and filtered [40] to increase signal-to-noise ratio. See also the Supplementary Information for the full set of differential interferograms.

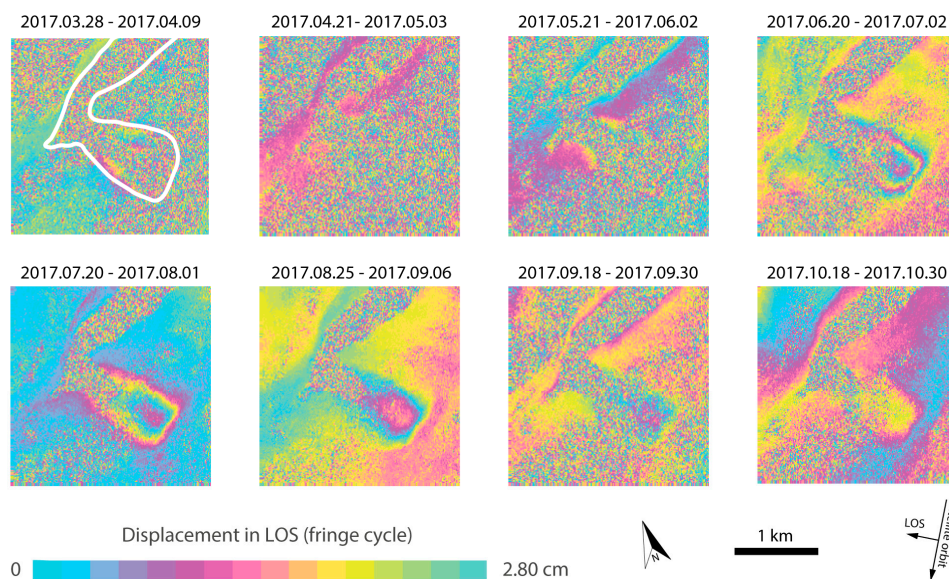


Figure 3. Selection of the Sentinel-1 (track 66, descending orbit) differential interferograms with 12-days temporal separation over the area of Moosfluh rock slope instability for the period March–October 2017. Time of acquisition for each SAR image pair analyzed is provided in the format YYYY.MM.DD. White the boundary in the upper left interferogram delineates the approximate area of the Aletsch glacier and Moosfluh slope instability (cf. Figure 1). Differential interferograms were generated by using a high resolution DEM (SwissALTI3D, 2 m GSD) and filtered [40] to increase signal-to-noise ratio. See also the Supplementary information for the full set of differential interferograms computed.

3.2. Results of DIC Analysis

Figure 4 shows the results obtained by applying the DIC approach on the S1 and S2 available datasets. The initial target was to achieve displacement measurements considering the minimum, however, this pairing strategy has provided unreliable measurements for both S1 and S2 dataset.

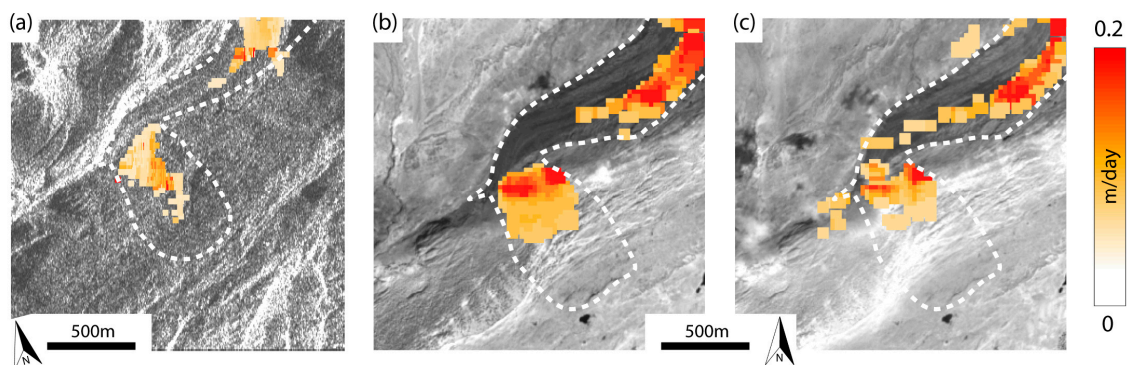


Figure 4. Best results obtained with the DIC analysis applied on the Sentinel-1 and Sentinel-2 datasets over the Moosfluh unstable slope. White boundary delineates the approximate area of the Aletsch glacier and Moosfluh slope instability (cf. Figure 1). (a) Resultant of the surface velocities measured across-track and along-track directions of Sentinel-1 in the period 8 June–18 October 2017. Background map is the SAR intensity for the SLC image 8 June 2017 (slant range oriented towards north); (b–c) Resultant of the horizontal surface velocities (E–N directions) measured on Sentinel-2 track R108 and R065 in the periods 19 July–17 October and 26 June–14 October 2017, respectively. Background maps are the surface reflectance for the images 19 July 2017 and 26 June 2017, respectively. Surface velocities in the lower portions of the Moosfluh instability and in the central part of the Great Aletsch glacier are well mapped by DIC. Inaccurate/outlier DIC values are masked out.

However, in the S1 pairs of 6- and 12-days the noise is very high. Instead, due to different acquisition parameters and/or atmospheric conditions (e.g., different sun angles, diffused and/or local cloud cover over Moosfluh, etc.), the number of S2 pairs suitable for DIC was severely reduced (see also Supplementary Materials, Table S4). For this reason, we have identified among the dataset image pairs providing reliable results, releasing the time constraint and targeting the average displacement rates. Several DIC attempts were performed and for both S1 and S2 data we obtained results in agreement with our ground observation, only with data pairs attaining temporal separations of several months. In Figure 4a, we show the results for a S1 pair spanning the summer period between June and October 2017. In the lower portions of the Moosfluh slope, decorrelated in the results obtained with standard DInSAR (see Section 3.1), the DIC results show large surface velocities (up to 0.15 m/day). This is in agreement with the DIC results obtained on the two S2 tracks, with values reaching up to 0.2 m/d in the portions near to the glacier tongue. Differences in surface displacement rates and their areal distribution between S1 and S2 DIC results can be observed due to different noise levels in the source imagery and/or also due to the different acquisition geometries (~40 degrees from vertical looking angle for S1, almost nadir for S2).

4. Discussion

When slope deformation suddenly increases, serious concerns are posed to elements at risk, such as population and/or infrastructures located within the area of influence of a potential landslide event [41]. For this reason, the selection of monitoring approaches aimed at managing the critical scenarios is crucial [42]. Spaceborne and airborne remote sensing data are usually exploited to identify and/or map areas showing signs of slope activity and threatened more as a long term planning tool, while ground based monitoring technologies are favored in case of Early Warning Systems aimed at providing timely information during the ultimate stages towards failure. Advances in spaceborne technology, particularly connected with the advent of the ESA Copernicus program, have pushed forward the idea of using satellite imagery also for the systematic and/or near-real-time monitoring of accelerated slope deformation. As far as Sentinel-1 data are concerned, Intrieri et al. [26] have used DInSAR time series after the occurrence of the Maoxian landslide event (Sichuan province, China), suggesting that acquisitions with a short revisiting time could be used not only as a tool for mapping unstable areas, but also for systematic landslide monitoring. In addition, Moretto et al. [43] have explored the possibility to use DInSAR time series to monitor landslide in pre-failure stages by simulating accelerated slope deformation over more than 50 landslide events as they would be acquired from past, actual, and future constellations of SAR satellites, including the Sentinel-1. They concluded that, based on Sentinel-1 acquisition parameters, phase ambiguity and revisit time limitations would have allowed to follow the evolution towards failure only for a minor portion of the analyzed dataset. Recently, Carlà et al. [44] have performed a retrospective analysis of a slope failure in an open-pit mine by combining ground-based radar and Sentinel-1 data, concluding that the shortened revisit time of modern satellites offers the opportunity to overcome problems related to high deformation gradients and thus help to identify and characterize impending slope failures. For what concerns Sentinel-2 data, Stumpf et al. [20] have developed a multi pairwise image correlation approach to detect and monitor surface displacement due to slope instability over large areas. They concluded that a systematic implementation of their approach could potentially allow sampling seasonal dynamics at the slope scale (i.e., accelerations due to ground water table variations associated to rainfall and/or snowmelt).

In this work, we aimed at conveying additional indications to this topic. Differently from previous studies, we attempt to leverage on the Sentinels during the critical phase (still ongoing at the time of writing), i.e., before and not after a major failure occurrence. We have processed Sentinel-1 and Sentinel-2 data available over the Moosfluh DSGSD, i.e., the most active and large DSGSD in the European Alps (150–200 millions of cubic meters). Even though we expect that only the lower part of the Moosfluh instability could fail catastrophically, this would be one of the largest rock slope failure events in the Alps since Vajont. In September 2016, large portions of the slope have shown signs of

accelerated surface deformation [28], suggesting a potential transition from block toppling into sliding and possibly into a kind of tertiary creep stage [29]. Our results show that differential interferograms of Sentinel-1 data with temporal separation of 6- and 12-days well image the spatial and temporal evolution of the deformation affecting the upper portions of the Moosfluh slope starting from the end of May until end of October 2017.

In Figure 5 we compare the average velocities retrieved from DInSAR versus measurements obtained from two ground based points systematically monitored since 2013 [1]. From the time series we note that the highest surface velocities in the upper portion of the slope (p35 in Figure 5) reached up to 0.012 m/day at the end of March. However, during this period, rapid surface changes due to snow melt affect the signal coherence, and thus hinders DInSAR analyses to catch such acceleration despite surface velocities would be still free from phase ambiguities. Starting from the middle of May (snow completely melted) velocity values become compatible to ground measurements. Slight differences between measurements are likely related to intrinsic DInSAR limitations (e.g., atmospheric phase screen), as well as by the fact that measurements at p35 are extremely local while DInSAR measurements are the average over the upper portions of Moosfluh. For what concerns the lower portions of the slope, we have shown that they are affected by low signal coherence during the whole observation period. Indeed, ground velocities affecting this area are already high at the beginning of the observation period (around 0.04 m/day at p75 in March, see Figure 5), and reach their climax at the beginning of September (0.25 m/day). Stacking the interferogram results to increase the signal-to-noise ratio (see Supplementary Material, Figure S3), as well as performing advanced DInSAR to derive time series [45–48], is not helpful in this case, because these approaches rely on stable signal coherence over the temporal windows of analysis.

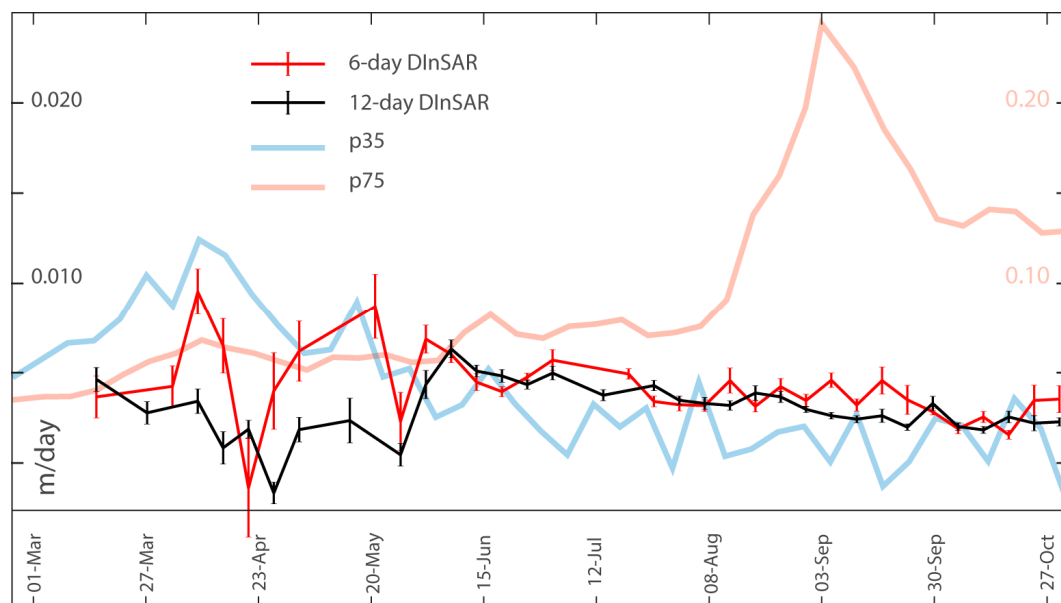


Figure 5. Comparison of DInSAR vs. ground measurements of surface velocities at Moosfluh rock slope instability during the period March–October 2017. DInSAR velocities are the average LOS displacements measured in the upper portions of Moosfluh. Error bars show standard deviations. The point p35 is located in the upper portion of the slope, while p75 on the lower portions (see geographic location in Figure 1). Ground measurements are projected towards the satellite LOS. Note: velocities of p75 are one order of magnitude higher, values are on the right y-axis.

We have shown that DIC methods can be used to take advantage of the amplitude information contained in the satellite SAR images. This approach is similar to what is proposed in other geohazards scenarios, where the combined use of satellite SAR phase and amplitude has increased the possibility

to measure and better interpret the surface deformation field [49,50]. Our results for Moosfluh suggest that DIC is particularly convenient to map the area affected by large slope deformation as well as to obtain fairly accurate surface velocities over selected time periods. Indeed, average velocities obtained from DIC on S1 and S2 data are well in agreement with values at p75 for the same time frame (see Figures 4 and 5). Although, we have also found that measurements obtained on the shortest possible revisit time (6-days for S1 and 10-days S2) are not suitable to monitor the evolution of surface displacements in critical scenarios where accurate monitoring is necessary. Advanced methodologies developed to combine multiple image pairs can only slightly improve the accuracy of DIC, because the main limitation is connected to the coarse GSD. The velocities observed at the Moosfluh DSGSD in fall 2016 and 2017 (0.2–0.8 m/day) are substantially bigger than most early warning threshold of past rock slope failures (e.g., 1 mm/day to 5 mm/h at the Preonzo instability complex of 0.22 millions of cubic meters, [2].) For smaller rock slope instabilities, the GSD might become a more critical parameter. By using of spaceborne data acquired with smaller GSD, accuracies of DIC results increase (see also Supplementary Materials, Figure S4), however, revisit times for these satellites, as well as data access is not straightforward as for the Sentinels. Thus, systematic monitoring would be probably possible only at specific sites while hindered elsewhere. Moreover, considering optical/multispectral sensors, the problem of atmospheric disturbances (both regional or at the scale of the slope) remains.

Ground-Based Remote Sensing as a Complement in Critical Scenarios?

Systematic monitoring of surface deformation performed with in-situ methods can also be complemented with terrestrial remote sensing, including ground based radar and optical imagery acquisitions [44,51–54]. These techniques are particularly convenient when the area of investigation has some access limitations due to high rates of surface deformation (e.g., formation of open fractures and increased rock fall activity). Moreover, spatial coverage of measurements is higher compared with in-situ measurements (usually point measurements), while temporal resolution and accuracies are comparable [51,55]. In Figure 6 we show the results obtained by using two different ground based remote sensing instruments to catch the large deformation occurring in the lower portions of the Moosfluh instability. The first one is a portable real aperture radar interferometer (Gamma Portable Radar Interferometer, GPRI), which is used to perform ad-hoc surveys of surface deformation in high alpine environments [56,57]. On 28 September 2017, we flew with helicopter on a convenient location to gain a complete view of the Moosfluh instability (see Figure 1). Radar acquisitions were performed every minute, and differential interferograms were stacked to obtain average surface velocities (in the sensor's LOS) over the entire period of acquisition (see Figure 6, left). The results show a clear representation of the most active portions of the Moosfluh rock slope, with values well in agreement with independent measurements (cf. Figure 5). The second instrument is a Mobotix M25 Time Lapse Camera (TLC, resolution 2592×1944 , i.e., 5Mpixel) installed in 2014 (see location in Figure 1) continuously acquiring optical imagery and since September 2016 directly transmitting the data every 10 min via GSM network to a remote server located at ETH Zurich. By applying the same Digital Image Correlation presented in Section 2.2 on a pair of TLC pictures (26 September and 28 September 2017), we retrieved comparable surface velocities as obtained from GPRI, although DIC measurements are in the camera view plane (i.e., almost orthogonal to the GPRI line of sight). These results demonstrate that both radar and optical ground based instruments may help gaining information within minutes over the entire slope affected surface deformation, and thus more suitable to obtain indications about spatial and temporal changes potentially leading to slope failure events.

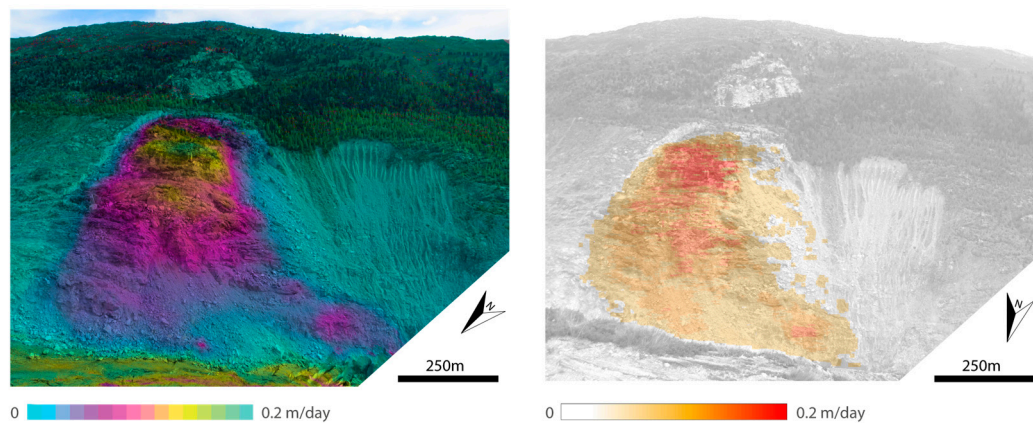


Figure 6. Surface velocity at Moosfluh measured with ground based remote sensing methods. **(Left)** GPR interferograms (stack of 1 min interferograms over 8 h) performed on 28 September 2017. **(Right)** Average velocity obtained applying DIC on time lapse camera data (image pair 26–28 September 2018) acquired from Driest (see camera location in Figure 1). Unreliable and/or outlier DIC values are masked out. The large deformation occurring in the lower portions of the Moosfluh slope is well mapped from both techniques in a short temporal frame, and average velocities are in agreement with independent ground measurements (cf. Figure 5, p75).

5. Conclusions

To evaluate the failure potential of active rock slope instabilities, a fundamental understanding of the predisposing factors and physical processes driving the slope movements and accelerations is essential [58,59]. This process understanding depends on high-resolution spatial and temporal records of slope displacements and the corresponding driving forces, such as pore pressure from rainfall and snow melt, surface temperature or glacial retreat. Without this background knowledge, interpretation of slope displacement histories, landslide hazards and risks, and predictions of the time-of-failure remain purely empirical and unreliable [60]. Models of failure forecast purely driven by observations, e.g., the inverse velocity method, might indicate a catastrophic failure potential of the entire slope, however, failure might not occur or only at minor portions [61]. These principles apply to all monitoring methods, however, satellite based measurements of surface deformation, both from optical and radar sensors, present additional intrinsic limitations. Here we have shown that when considering the ESA Sentinels over active slopes, surface velocities are often too high for DInSAR analyses but below sensitivity thresholds of Digital Image Correlation approaches, thus, extreme caution must be taken when using this data for systematic monitoring applications as well as in their interpretation. At the current stage, only ground based monitoring instruments, including standard in-situ and remote sensing methods, can ensure systematic and accurate displacement measurements, as well as the very high temporal resolution needed for process understanding, real time monitoring, and/or forecasting of catastrophic slope failure events.

Supplementary Materials: The following are available online at <http://www.mdpi.com/2072-4292/10/5/672/s1>, Figure S1: Field pictures of the tensile fractures formed during the 2016 crisis at the Moosfluh slope. Figure S2: Full set of Sentinel-1 differential interferograms processed in this study, Figure S3: Stack of differential interferograms with 6-days and 12-days temporal separation, Figure S4: Digital Image Correlation results obtained with ALOS Palsar-2, Table S1: Sentinel-1 dataset, Table S2: Sentinel-2 dataset, Table S3: List of differential interferograms processed, Table S4: Visibility of the area of study in the Sentinel-2 dataset.

Author Contributions: A.M. designed the experiments, analyzed the results, and wrote the paper; P.K. performed the Sentinel-1 DInSAR processing. T.S. and A.M. made the DIC analyses. R.C. accomplished the GPR campaign and processed the data acquired. S.L. provided details for the introduction and discussion sections. All authors contributed to the manuscript revision.

Acknowledgments: We thank the Editor F. Catani and two anonymous reviewers for valuable comments.

Conflicts of Interest: The authors declare no conflict of interest.

References

- Loew, S.; Gischig, V.; Glueer, F.; Seifert, R.; Moore, J.R. Multidisciplinary monitoring of progressive failure processes in brittle rock slopes. In *Rock Mechanics and Engineering Volume 4: Excavation, Support and Monitoring*; CRC Press: London, UK, 2017; Volume 4, pp. 629–662.
- Loew, S.; Gschwind, S.; Gischig, V.; Keller-Signer, A.; Valenti, G. Monitoring and early warning of the 2012 Preonzo catastrophic rockslope failure. *Landslides* **2017**, *14*, 141–154. [[CrossRef](#)]
- Calò, F.; Ardizzone, F.; Castaldo, R.; Lollino, P.; Tizzani, P.; Guzzetti, F.; Lanari, R.; Angeli, M.-G.; Pontoni, F.; Manunta, M. Enhanced landslide investigations through advanced DInSAR techniques: The Ivancich case study, Assisi, Italy. *Remote Sens. Environ.* **2014**, *142*, 69–82. [[CrossRef](#)]
- Meisina, C.; Zucca, F.; Notti, D.; Colombo, A.; Cucchi, A.; Savio, G.; Giannico, C.; Bianchi, M. Geological interpretation of PSInSAR Data at regional scale. *Sensors* **2008**, *8*, 7469–7492. [[CrossRef](#)] [[PubMed](#)]
- Herrera, G.; Gutiérrez, F.; García-Davalillo, J.C.; Guerrero, J.; Notti, D.; Galve, J.P.; Fernández-Merodo, J.A.; Cooksley, G. Multi-sensor advanced DInSAR monitoring of very slow landslides: The Tena Valley case study (Central Spanish Pyrenees). *Remote Sens. Environ.* **2013**, *128*, 31–43. [[CrossRef](#)]
- Strozzi, T.; Delaloye, R.; Kääh, A.; Ambrosi, C.; Perruchoud, E.; Wegmüller, U. Combined observations of rock mass movements using satellite SAR interferometry, differential GPS, airborne digital photogrammetry, and airborne photography interpretation. *J. Geophys. Res.* **2010**, *115*. [[CrossRef](#)]
- Bürgmann, R.; Rosen, P.A.; Fielding, E.J. Synthetic aperture radar interferometry to measure Earth’s surface topography and its deformation. *Annu. Rev. Earth Planet. Sci.* **2000**, *28*, 169–209. [[CrossRef](#)]
- Casu, F.; Manzo, M.; Lanari, R. A quantitative assessment of the SBAS algorithm performance for surface deformation retrieval from DInSAR data. *Remote Sens. Environ.* **2006**, *102*, 195–210. [[CrossRef](#)]
- Wasowski, J.; Bovenga, F. Investigating landslides and unstable slopes with satellite Multi Temporal Interferometry: Current issues and future perspectives. *Eng. Geol.* **2014**, *174*, 103–138. [[CrossRef](#)]
- Przyłucka, M.; Herrera, G.; Graniczny, M.; Colombo, D.; Béjar-Pizarro, M. Combination of Conventional and Advanced DInSAR to Monitor Very Fast Mining Subsidence with TerraSAR-X Data: Bytom City (Poland). *Remote Sens.* **2015**, *7*, 5300–5328. [[CrossRef](#)]
- Casu, F.; Manconi, A.; Pepe, A.; Lanari, R. Deformation Time-Series Generation in Areas Characterized by Large Displacement Dynamics: The SAR Amplitude Pixel-Offset SBAS Technique. *IEEE Trans. Geosci. Remote Sens.* **2011**, *49*, 2752–2763. [[CrossRef](#)]
- Manconi, A.; Casu, F.; Ardizzone, F.; Bonano, M.; Cardinali, M.; De Luca, C.; Gueguen, E.; Marchesini, I.; Parise, M.; Vennari, C.; et al. Brief communication: Rapid mapping of event landslides: the 3 December 2013 Montescaglioso landslide (Italy). *Nat. Hazards Earth Syst. Sci. Discuss.* **2014**, *2*, 1465–1479. [[CrossRef](#)]
- Singleton, A.; Li, Z.; Hoey, T.; Muller, J.-P. Evaluating sub-pixel offset techniques as an alternative to D-InSAR for monitoring episodic landslide movements in vegetated terrain. *Remote Sens. Environ.* **2014**, *147*, 133–144. [[CrossRef](#)]
- Sun, L.; Muller, J.-P.; Chen, J. Time Series Analysis of Very Slow Landslides in the Three Gorges Region through Small Baseline SAR Offset Tracking. *Remote Sens.* **2017**, *9*, 1314. [[CrossRef](#)]
- Cai, J.; Wang, C.; Mao, X.; Wang, Q. An Adaptive Offset Tracking Method with SAR Images for Landslide Displacement Monitoring. *Remote Sens.* **2017**, *9*, 830. [[CrossRef](#)]
- Elefante, S.; Manconi, A.; Bonano, M.; De Luca, C.; Casu, F. Three-dimensional ground displacements retrieved from SAR data in a landslide emergency scenario. In Proceedings of the 2014 IEEE International on Geoscience and Remote Sensing Symposium (IGARSS), Quebec City, QC, Canada, 13–18 July 2014; pp. 2400–2403.
- Gorelick, N.; Hancher, M.; Dixon, M.; Ilyushchenko, S.; Thau, D.; Moore, R. Google Earth Engine: Planetary-scale geospatial analysis for everyone. *Remote Sens. Environ.* **2017**. [[CrossRef](#)]
- Wulder, M.A.; White, J.C.; Loveland, T.R.; Woodcock, C.E.; Belward, A.S.; Cohen, W.B.; Fosnight, E.A.; Shaw, J.; Masek, J.G.; Roy, D.P. The global Landsat archive: Status, consolidation, and direction. *Remote Sens. Environ.* **2016**, *185*, 271–283. [[CrossRef](#)]

19. Scambos, T.A.; Dutkiewicz, M.J.; Wilson, J.C.; Bindschadler, R.A. Application of image cross-correlation to the measurement of glacier velocity using satellite image data. *Remote Sens. Environ.* **1992**, *42*, 177–186. [[CrossRef](#)]
20. Stumpf, A.; Malet, J.-P.; Delacourt, C. Correlation of satellite image time-series for the detection and monitoring of slow-moving landslides. *Remote Sens. Environ.* **2017**, *189*, 40–55. [[CrossRef](#)]
21. Bennett, G.L.; Roering, J.J.; Mackey, B.H.; Handwerker, A.L.; Schmidt, D.A.; Guillod, B.P. Historic drought puts the brakes on earthflows in Northern California. *Geophys. Res. Lett.* **2016**, *43*, 5725–5731. [[CrossRef](#)]
22. Barra, A.; Solari, L.; Béjar-Pizarro, M.; Monserrat, O.; Bianchini, S.; Herrera, G.; Crosetto, M.; Sarro, R.; González-Alonso, E.; Mateos, R.M.; et al. A Methodology to Detect and Update Active Deformation Areas Based on Sentinel-1 SAR Images. *Remote Sens.* **2017**, *9*, 1002. [[CrossRef](#)]
23. Calvellido, M.; Peduto, D.; Arena, L. Combined use of statistical and DInSAR data analyses to define the state of activity of slow-moving landslides. *Landslides* **2017**, *14*, 473–489. [[CrossRef](#)]
24. Crosta, G.B.; Frattini, P.; Agliardi, F. Deep seated gravitational slope deformations in the European Alps. *Tectonophysics* **2013**, *605*, 13–33. [[CrossRef](#)]
25. Giordan, D.; Allasia, P.; Manconi, A.; Baldo, M.; Santangelo, M.; Cardinali, M.; Corazza, A.; Albanese, V.; Lollino, G.; Guzzetti, F. Morphological and kinematic evolution of a large earthflow: The Montaguto landslide, southern Italy. *Geomorphology* **2013**, *187*, 61–79. [[CrossRef](#)]
26. Intrieri, E.; Raspini, F.; Fumagalli, A.; Lu, P.; Conte, S.D.; Farina, P.; Allievi, J.; Ferretti, A.; Casagli, N. The Maoxian landslide as seen from space: detecting precursors of failure with Sentinel-1 data. *Landslides* **2017**, 1–11. [[CrossRef](#)]
27. Aschbacher, J.; Milagro-Pérez, M.P. The European Earth monitoring (GMES) programme: Status and perspectives. *Remote Sens. Environ.* **2012**, *120*, 3–8. [[CrossRef](#)]
28. Kos, A.; Amann, F.; Strozzi, T.; Delaloye, R.; von Ruetten, J.; Springman, S. Contemporary glacier retreat triggers a rapid landslide response, Great Aletsch Glacier, Switzerland. *Geophys. Res. Lett.* **2016**, *43*, 12466–12474. [[CrossRef](#)]
29. Rosser, N.; Lim, M.; Petley, D.; Dunning, S.; Allison, R. Patterns of precursory rockfall prior to slope failure. *J. Geophys. Res. Earth Surf.* **2007**, *112*, F04014. [[CrossRef](#)]
30. Torres, R.; Snoeij, P.; Geudtner, D.; Bibby, D.; Davidson, M.; Attema, E.; Potin, P.; Rommen, B.; Flouy, N.; Brown, M.; et al. GMES Sentinel-1 mission. *Remote Sens. Environ.* **2012**, *120*, 9–24. [[CrossRef](#)]
31. Zan, F.D.; Guarnieri, A.M.M. TOPSAR: Terrain Observation by Progressive Scans. *IEEE Trans. Geosci. Remote Sens.* **2006**, *44*, 2352–2360. [[CrossRef](#)]
32. Drusch, M.; Del Bello, U.; Carlier, S.; Colin, O.; Fernandez, V.; Gascon, F.; Hoersch, B.; Isola, C.; Laberinti, P.; Martimort, P.; et al. Sentinel-2: ESA's Optical High-Resolution Mission for GMES Operational Services. *Remote Sens. Environ.* **2012**, *120*, 25–36. [[CrossRef](#)]
33. Crosta, G.B.; di Prisco, C.; Frattini, P.; Frigerio, G.; Castellanza, R.; Agliardi, F. Chasing a complete understanding of the triggering mechanisms of a large rapidly evolving rockslide. *Landslides* **2014**, *11*, 747–764. [[CrossRef](#)]
34. Wegnüller, U.; Werner, C.; Strozzi, T.; Wiesmann, A.; Frey, O.; Santoro, M. Sentinel-1 Support in the GAMMA Software. *Procedia Comput. Sci.* **2016**, *100*, 1305–1312. [[CrossRef](#)]
35. Pritchard, M.E. InSAR, a tool for measuring Earth's surface deformation. *Phys. Today* **2006**, *59*, 68–69. [[CrossRef](#)]
36. Heid, T.; Käab, A. Evaluation of existing image matching methods for deriving glacier surface displacements globally from optical satellite imagery. *Remote Sens. Environ.* **2012**, *118*, 339–355. [[CrossRef](#)]
37. Guizar-Sicairos, M.; Thurman, S.T.; Fienup, J.R. Efficient subpixel image registration algorithms. *Opt. Lett.* **2008**, *33*, 156–158. [[CrossRef](#)] [[PubMed](#)]
38. Wang, Z.; Kieu, H.; Nguyen, H.; Le, M. Digital image correlation in experimental mechanics and image registration in computer vision: Similarities, differences and complements. *Opt. Lasers Eng.* **2015**, *65*, 18–27. [[CrossRef](#)]
39. Leprince, S.; Barbot, S.; Ayoub, F.; Avouac, J.-P. Automatic and Precise Orthorectification, Coregistration, and Subpixel Correlation of Satellite Images, Application to Ground Deformation Measurements. *IEEE Trans. Geosci. Remote Sens.* **2007**, *45*, 1529–1558. [[CrossRef](#)]
40. Goldstein, R.M.; Werner, C.L. Radar interferogram filtering for geophysical applications. *Geophys. Res. Lett.* **1998**, *25*, 4035–4038. [[CrossRef](#)]

41. Lollino, G.; Manconi, A.; Giordan, D.; Allasia, P.; Baldo, M. Infrastructure in Geohazard Contexts: The Importance of Automatic and Near-Real-Time Monitoring. In *Environmental Security of the European Cross-Border Energy Supply Infrastructure*; Culshaw, M.G., Osipov, V.I., Booth, S.J., Victorov, A.S., Eds.; Springer: Dordrecht, The Netherlands, 2015; pp. 73–89. ISBN 978-94-017-9537-1.
42. Manconi, A. Monitoring. In *Encyclopedia of Engineering Geology*; Bobrowsky, P.T., Marker, B., Eds.; Springer: Cham, Switzerland, 2016; pp. 1–8. ISBN 978-3-319-12127-7.
43. Moretto, S.; Bozzano, F.; Esposito, C.; Mazzanti, P.; Rocca, A. Assessment of Landslide Pre-Failure Monitoring and Forecasting Using Satellite SAR Interferometry. *Geosciences* **2017**, *7*, 36. [[CrossRef](#)]
44. Carlà, T.; Farina, P.; Intrieri, E.; Ketizmen, H.; Casagli, N. Integration of ground-based radar and satellite InSAR data for the analysis of an unexpected slope failure in an open-pit mine. *Eng. Geol.* **2018**, *235*, 39–52. [[CrossRef](#)]
45. Berardino, P.; Fornaro, G.; Lanari, R.; Sansosti, E. A new algorithm for surface deformation monitoring based on small baseline differential SAR interferograms. *IEEE Trans. Geosci. Remote Sens.* **2002**, *40*, 2375–2383. [[CrossRef](#)]
46. Ferretti, A.; Prati, C.; Rocca, F. Permanent scatterers in SAR interferometry. *IEEE Trans. Geosci. Remote Sens.* **2001**, *39*, 8–20. [[CrossRef](#)]
47. Hooper, A. A multi-temporal InSAR method incorporating both persistent scatterer and small baseline approaches. *Geophys. Res. Lett.* **2008**, *35*, L16302. [[CrossRef](#)]
48. Ferretti, A.; Fumagalli, A.; Novali, F.; Prati, C.; Rocca, F.; Rucci, A. A New Algorithm for Processing Interferometric Data-Stacks: SqueeSAR. *IEEE Trans. Geosci. Remote Sens.* **2011**, *49*, 3460–3470. [[CrossRef](#)]
49. Manconi, A.; Casu, F. Joint analysis of displacement time series retrieved from SAR phase and amplitude: Impact on the estimation of volcanic source parameters. *Geophys. Res. Lett.* **2012**, *39*, GL052202. [[CrossRef](#)]
50. Solari, L.; Raspini, F.; Soldato, M.D.; Bianchini, S.; Ciampalini, A.; Ferrigno, F.; Tucci, S.; Casagli, N. Satellite radar data for back-analyzing a landslide event: the Ponzano (Central Italy) case study. *Landslides* **2018**, *15*, 773–782. [[CrossRef](#)]
51. Travelletti, J.; Delacourt, C.; Allemand, P.; Malet, J.-P.; Schmittbuhl, J.; Toussaint, R.; Bastard, M. Correlation of multi-temporal ground-based optical images for landslide monitoring: Application, potential and limitations. *ISPRS J. Photogramm. Remote Sens.* **2012**, *70*, 39–55. [[CrossRef](#)]
52. Monserrat, O.; Crosetto, M.; Luzi, G. A review of ground-based SAR interferometry for deformation measurement. *ISPRS J. Photogramm. Remote Sens.* **2014**, *93*, 40–48. [[CrossRef](#)]
53. Giordan, D.; Allasia, P.; Dematteis, N.; Dell’Anese, F.; Vagliasindi, M.; Motta, E. A Low-Cost Optical Remote Sensing Application for Glacier Deformation Monitoring in an Alpine Environment. *Sensors* **2016**, *16*, 1750. [[CrossRef](#)] [[PubMed](#)]
54. Bardi, F.; Raspini, F.; Frodella, W.; Lombardi, L.; Nocentini, M.; Gigli, G.; Morelli, S.; Corsini, A.; Casagli, N. Monitoring the Rapid-Moving Reactivation of Earth Flows by Means of GB-InSAR: The April 2013 Capriglio Landslide (Northern Apennines, Italy). *Remote Sens.* **2017**, *9*, 165. [[CrossRef](#)]
55. Caduff, R.; Schlunegger, F.; Kos, A.; Wiesmann, A. A review of terrestrial radar interferometry for measuring surface change in the geosciences. *Earth Surf. Process. Landf.* **2015**, *40*, 208–228. [[CrossRef](#)]
56. Werner, C.; Strozzi, T.; Wiesmann, A.; Wegmüller, U. A ground-based real-aperture radar instrument for differential interferometry. In Proceedings of the 2009 IEEE on Radar Conference, Pasadena, CA, USA, 4–8 May 2009; pp. 1–4.
57. Werner, C.; Wiesmann, A.; Strozzi, T.; Kos, A.; Caduff, R.; Wegmüller, U. The GPRI multi-mode differential interferometric radar for ground-based observations. In Proceedings of the EUSAR 2012 on 9th European Conference on Synthetic Aperture Radar, Nuremberg, Germany, 23–26 April 2012; pp. 304–307.
58. Grämiger, L.M.; Moore, J.R.; Gischig, V.S.; Ivy-Ochs, S.; Loew, S. Beyond debuttressing: Mechanics of paraglacial rock slope damage during repeat glacial cycles. *J. Geophys. Res. Earth Surf.* **2017**, *122*, 1004–1036. [[CrossRef](#)]
59. Loew, S.; Gischig, V.; Moore, J.R.; Keller-Signer, A. Monitoring of potentially catastrophic rockslides. In Proceedings of the 11th International and 2nd North American Symposium on Landslides and Engineered Slopes on Landslides and Engineered Slopes: Protecting society through improved understanding, Banff, AB, Canada, 3–8 June 2012; pp. 101–116.
60. Petley, D.N.; Mantovani, F.; Bulmer, M.H.; Zannoni, A. The use of surface monitoring data for the interpretation of landslide movement patterns. *Geomorphology* **2005**, *66*, 133–147. [[CrossRef](#)]

61. Manconi, A.; Giordan, D. Landslide early warning based on failure forecast models: the example of the Mt. de La Saxe rockslide, northern Italy. *Nat. Hazards Earth Syst. Sci.* **2015**, *15*, 1639–1644. [[CrossRef](#)]



© 2018 by the authors. Licensee MDPI, Basel, Switzerland. This article is an open access article distributed under the terms and conditions of the Creative Commons Attribution (CC BY) license (<http://creativecommons.org/licenses/by/4.0/>).